

# Impact of surface-polish on the angular and wavelength dependence of fiber focal ratio degradation

Arthur D. Eigenbrot, Matthew A. Bershady, Corey M. Wood

University of Wisconsin, 475 N. Charter St, Madison WI, 53706, USA

## ABSTRACT

We present measurements of how multimode fiber focal-ratio degradation (FRD) and throughput vary with levels of fiber surface polish from 60 to 0.5 micron grit. Measurements used full-beam and laser injection methods at wavelengths between 0.4 and 0.8 microns on 17 meter lengths of Polymicro FBP 300 and 400  $\mu\text{m}$  core fiber. Full-beam injection probed input focal-ratios between  $f/3$  and  $f/13.5$ , while laser injection allowed us to isolate FRD at discrete injection angles up to 17 degrees ( $f/1.6$  marginal ray). We find (1) FRD effects decrease as grit size decreases, with the largest gains in beam quality occurring at grit sizes above 5  $\mu\text{m}$ ; (2) total throughput increases as grit size decreases, reaching 90% at 790 nm with the finest polishing levels; (3) total throughput is higher at redder wavelengths for coarser polishing grit, indicating surface-scattering as the primary source of loss. We also quantify the angular dependence of FRD as a function of polishing level. Our results indicate that a commonly adopted micro-bending model for FRD is a poor descriptor of the observed phenomenon.

**Keywords:** multi-mode fibers, fiber optics, focal ratio degradation

## 1. INTRODUCTION

Multimode optical fibers provide the most cost-effective coupling between telescopes and spectrographs that allow spectrographs to be placed in stable environments. However, these fiber optics contribute to light loss from attenuation within the fiber material and surface-scattering of their ends, and increase entropy in the optical beam. The latter is referred to as focal ratio degradation (FRD), whereby light injected into a fiber at a particular  $f$ -ratio emerges at a faster (smaller)  $f$ -ratio. Ever since the first efforts to characterize FRD in astronomical applications<sup>1</sup> astronomers have attempted to understand its cause(s) in the hope to lessen its effects.<sup>2,3</sup> Microbends have historically been a favored culprit,<sup>2,4</sup> but recently it has been suggested<sup>5,6</sup> that scattering caused by surface-roughness on the fiber face contributes significantly to FRD.

We discuss the results of two experiments designed to measure how the amount of FRD depends on surface roughness, wavelength, and input angle. The experiments described here use both full-beam and laser injection methods<sup>2</sup> standard for FRD tests in astronomical applications. The full-beam method is useful for characterizing how a fiber would perform when fed by a telescope, and provides a straightforward way to compute practical metrics useful for designing spectroscopic instruments. The laser injection method allows light to be injected into the fiber at discrete input angles (compared to a filled ray-bundle cone). This angular dependence of scattering is a particularly sensitive diagnostic of the physical mechanisms responsible for FRD.

The method and results of our experiment of FRD dependence on surface roughness are presented in §2. Results for the wavelength dependence of FRD are reported in §2.4.2. The dependence of scattering on input angle is reported in §3, and the implications of our work are discussed in §4.

## 2. GRIT SIZE AND WAVELENGTH DEPENDENCE

### 2.1 Polishing Method

Our tests used Polymicro Technologies stepped-index broadband optical fibers, cut to  $\sim 17$  meters in length. FBP300330370 has core:clad:buffer diameters of 300:330:370  $\mu\text{m}$ , respectively; a second length of FBP400440480 has 400:440:480  $\mu\text{m}$  diameters. We mounted each fiber end into 0.25 inch cylindrical brass ferrules using Norland Optical Adhesive 61 ultraviolet-curing epoxy.

---

Correspondence to eigenbrot@astro.wisc.edu

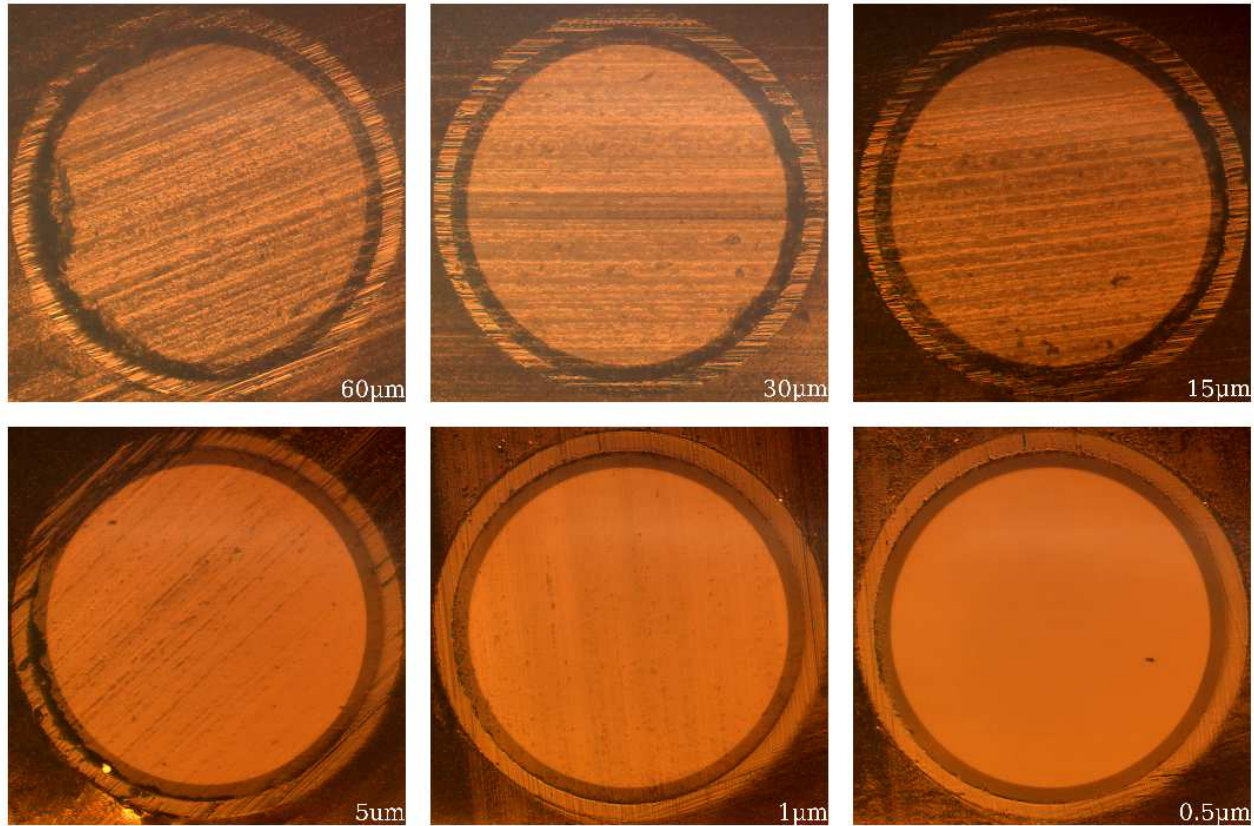


Figure 1. Images of the “test” surface of the fiber cable showing the appearance of the fiber face at each of the six stages of polishing. The number in the bottom right corner of each panel denotes the size of grit used. The fiber core diameter is  $300\mu\text{m}$ .

The experiment was designed to maintain one end of each fiber cable as a “control” surface, well-polished ( $0.5\ \mu\text{m}$ ) at the beginning of testing, and to use the other end of the fiber cable as the “test” surface, initially polished using a coarse grit and then re-polished with successively finer grit sizes after each measurement. For creating the progression of decreasing surface roughness we performed consecutive polishing steps on the test surface using silicon carbide lapping disks of 60, 30, 15, 5, and  $1\ \mu\text{m}$  grit as well as  $0.5\ \mu\text{m}$  grit aluminum oxide disks.

The fiber cable was polished using an Ultra Tec Manufacturing, Inc., ULTRAPOL 1200-series lapping machine. We considered a fiber surface to be adequately polished when, under visual inspection, surface grooves appeared to be relatively even across the face with very few surface features larger than the grit size used to polish the surface. We imaged each end of the fiber using a Newport Corporation F-ML1 fiber inspection microscope for magnification and a Motic Corporation Moticam 2300 CMOS detector. We took images after each polishing step in order to confirm that the test surface was adequately polished and that the control surface remained undamaged. We also captured images after each FRD measurement step in order to determine if the fiber faces had been damaged during handling, as any potential damage could affect the test results. A mosaic of images of the test surface, as seen after the FRD measurement at each grit size, is seen in Figure 1.

## 2.2 Data Collection

The experimental apparatus is a modified version of the far-field differential beam comparator using a double re-imaging system described in Crause et al. (2008),<sup>7</sup> which is based of the FRD test apparatus used to characterize the fibers of SPARSPAK.<sup>8</sup> The final collimating lens (L3 in Crause et al. (2008)<sup>7</sup>) was replaced with a Canon

$f/1.2$  camera lens to eliminate ghost images caused by very fast output beams. Stray light was further reduced by covering everything downstream of the focus plane with a black photographer’s cloth. The fiber input stage was replaced with a highly stable, purpose-built three-axis translation stage that ensures the fiber face is telecentric to within  $0.01^\circ$ . Finally, a filter magazine was added to the pinhole assembly to facilitate the rapid changing of filters.

Basic operation involves recording data from two imaging modes; the far-field fiber output, and the far-field image of the direct beam. The level of FRD is then computed by comparing the two modes. Examples of these images are shown in Figure 2, illustrating the increasing impact of FRD at slower beam-speeds. Data were taken in three filters: Johnson I and B and Stromgren  $y$ , with central wavelengths of 790 nm, 440 nm, 551 nm, and widths of  $\Delta\lambda/\lambda = 0.22, 0.19, 0.045$ , respectively; four  $f$ -ratios ( $f/3, f/4.2, f/6.3$ , and  $f/13.5$ ); and five polish levels (60, 30, 15, 5, and  $1 \mu\text{m}$ ). The range in  $f$ -ratios was chosen so that results are applicable to a wide range of telescope designs. The Wisconsin Indiana Yale NOAO (WIYN) 3.5m telescope has a  $f/6.3$  Nasmyth port; the Sloan Digital Sky Survey Telescope fibers are fed at  $f/5$ ; and the South African Large Telescope (SALT) feeds its prime focus instrument package at  $f/4.2$  (similar to the Hobby Eberly Telescope).

Throughput measurements require very precise knowledge of the intrinsic lamp output (the light input to the system). Experiments in lab showed that, while the stochastic variations of the lamp are negligible, there is a secular drift towards lower lamp output. Subsequent to the experiment reported here a photo-diode monitoring system has been implemented to correct for this trend. The data presented here accounted for this trend by: 1) taking a set of images for one filter with the fiber in place, 2) taking a set of direct beam images in the same filter, 3) repeating this alternating scheme until three groups of fiber images, separated by two groups of direct beam images were taken. This alternating fiber-direct-fiber scheme is used to remove stochastic lamp variability.

Images were cleaned of detector artifacts and combined to produce five images for each filter at each polish level: three fiber images and two direct beam images. Lamp variations were removed by using the three fiber images as data points to determine a lamp normalization (relative to the first fiber image) as a function of time. This function was then used to find normalizations for the direct beam images. The lamp was found to have no significant variation (10% of the shot noise) within the time required to take one set of data in a particular filter.

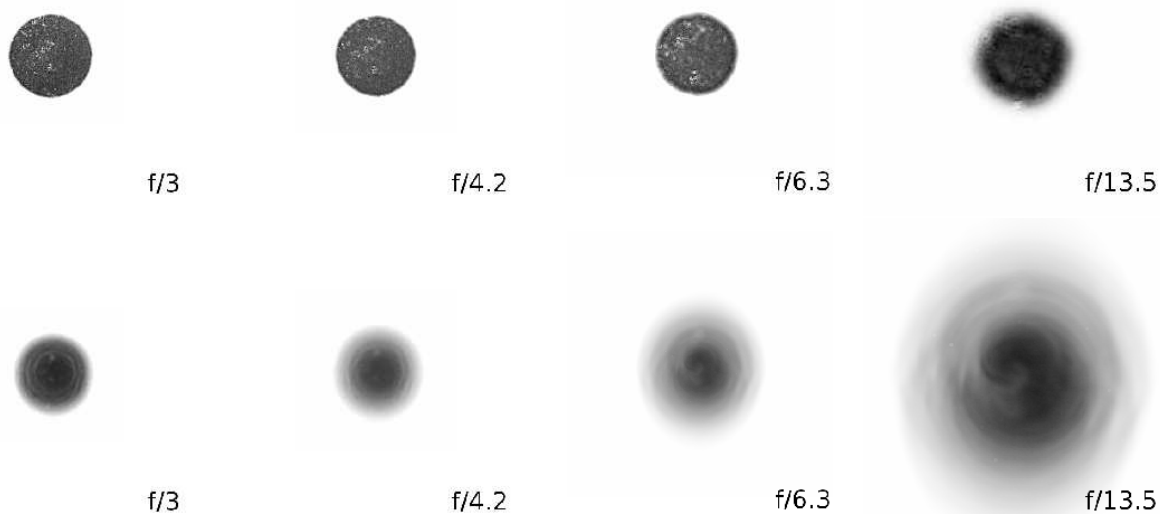


Figure 2. Far-field images of the direct-beam (top) and fiber-beam (bottom) outputs for all  $f$ -ratios tested. Data shown is at 551 nm for the FBP300330370 fiber, 17m in length. Direct and fiber beam images for a given  $f$ -ratio have identical spatial scales, and are adjusted such that the direct beam images are the same apparent size for all  $f$ -ratios.

### 2.3 Analysis

A custom data reduction pipeline was created to consistently and efficiently analyze the large volume of data associated with the multiple filters and polish levels. Analysis consisted of measuring the total light contained within annuli of constant width and increasing radius centered on the center of the beam. This information was then used to construct a curve of growth that shows the fractional encircled energy (EE) as a function of radius.

In addition to FRD, there are aberrations inherent in our test apparatus that will affect both the direct beam and fiber beam in the same way. To remove the effects of these aberrations the difference between the direct beam and a theoretical ideal beam (no aberrations) is computed and applied to both the fiber and direct beams; Crause et al. (2008)<sup>7</sup> provide a complete description of the method used. Once the corrections have been applied the only differences between the fiber and direct beams are caused by FRD.

### 2.4 Results

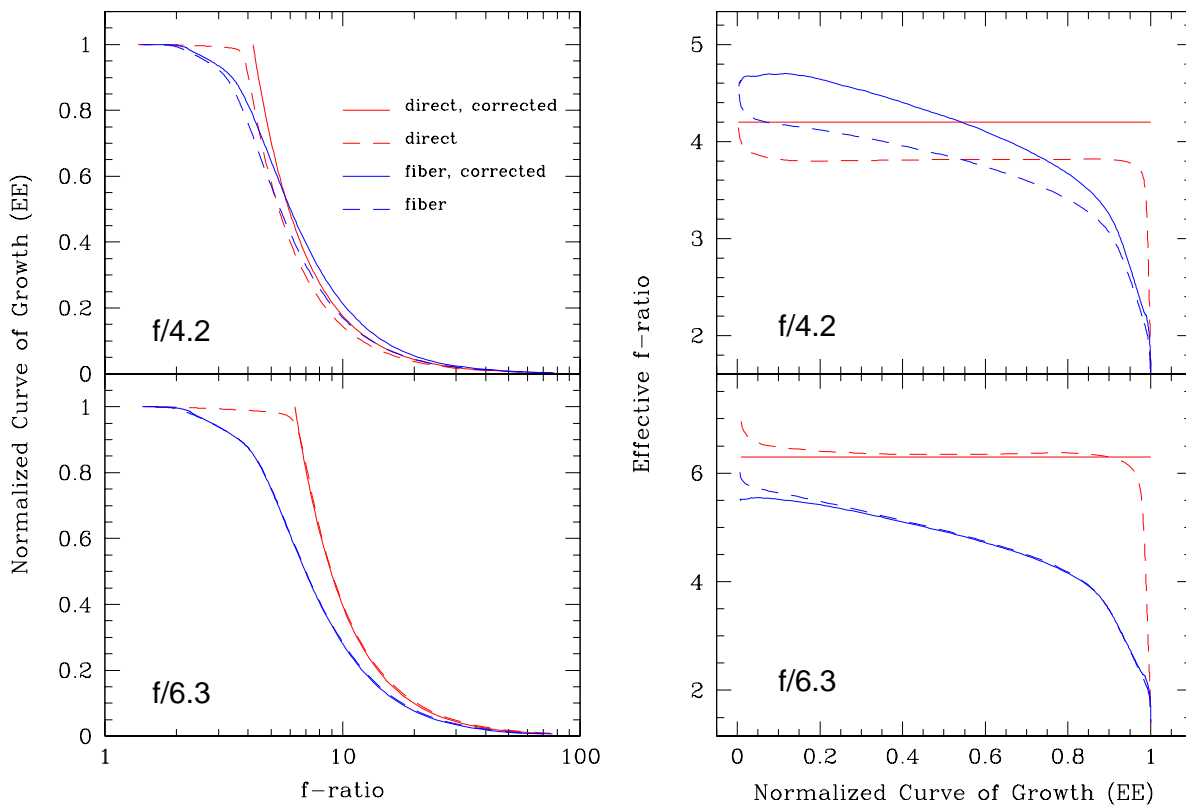


Figure 3. FRD effects at 551 nm,  $f/4.2$  and  $f/6.3$ , and with the output face polished to  $30\ \mu\text{m}$ . The left panels show enclosed energy (EE) as a function of  $f$ -ratio. The right panels show the effective  $f$ -ratio of a beam that captures a certain percentage of the total light (EE). Data is for the FBP300330370 fiber, 17m in length. A color version of this plot is available online.

Figure 3 shows a characteristic set of FRD analysis plots at a  $30\ \mu\text{m}$  end-polish at  $f/4.2$  and  $f/6.3$ . (See Figure 4 for more grit-sizes and §2.4.1 for discussion). The left panels, which consist of normalized curves of growth (COG) for both the direct and fiber beams, show how FRD scatters light out to larger radii. The dashed and solid lines are the data before and after the correction described above.<sup>7</sup>

The right panels plot the effective  $f$ -ratio as a function of EE. These plots only show information about relative light (re)distribution; they do not contain any information about total throughput. Where the fiber

curve intersects the ideal beam tells us what percentage of the original beam's information is being captured by a spectrograph with an  $f$ -ratio equal to that of the optics feeding the fibers. This plot can also be used to estimate how much faster a spectrograph would have to be to capture more of the input beam. For example, from figure 3 and for fibers polished to  $30\ \mu\text{m}$ , an  $f/4.2$  spectrograph only captures about 53% of the light fed into the fibers at  $f/4.2$ . If we wanted to capture 90% of the input light the spectrograph optics would need to be  $f/3.2$ .

### 2.4.1 Grit-size and $f$ -ratio Dependence

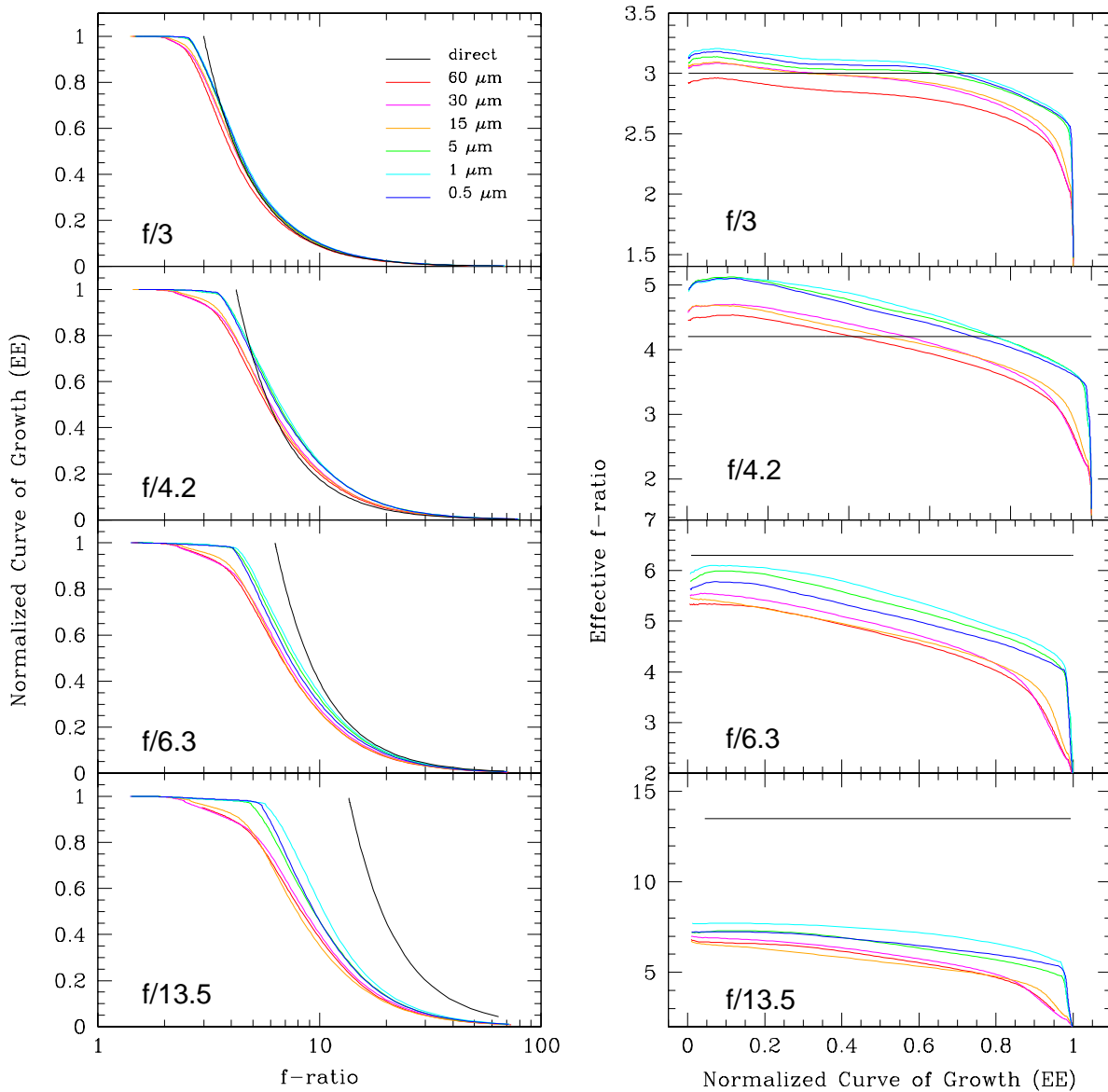


Figure 4. Dependence of FRD on polish grit size at 551 nm and all  $f$ -ratios measured for 17m of FBP300330370 fiber. A color version of this plot is available online.

The primary result of the experiment can be seen in figure 4, which shows FRD curves at one wavelength

(551 nm) and at all of the different end-polish levels and  $f$ -ratios. As expected, the effects of FRD improve as grit size decreases, but only to a point. There is steady improvement in output beam quality between 60  $\mu\text{m}$  and 15  $\mu\text{m}$ , a sharp improvement between 15  $\mu\text{m}$  and 5  $\mu\text{m}$ , and almost no improvement between 5  $\mu\text{m}$  and 0.5  $\mu\text{m}$ .

It is also worth noting that for certain combinations of input  $f$ -ratio and polish level there is a radius (output  $f$ -ratio) within which there is relatively *more* light in the fiber beam than in the direct beam. The explanation is straightforward: FRD scatters light from each input angle into both larger and smaller output angles. If the width of the scattering profile increases towards smaller angles (see §3) then more light is scattered out of these angles compared to larger angles. However, for a uniform input beam larger input angles contain more luminosity (because they contain larger annular areas) and so the amount of light scattered in from large angles will exceed the amount of light scattered out from small angles despite the wider scattering profile at small angles. In this case the fiber beam will have relatively more light at smaller angles than the direct beam, as seen in the plots for  $f/3$  and  $f/4.2$ . Conversely, there is some sufficiently large output angle that has significant scattering contributions from angles where there is no light in the input beam. At these output angles, the COG drops below the ideal beam, as observed.

It is well known that FRD changes with changing input  $f$ -ratio, increasing with slower beams (Ramsey 1988),<sup>9</sup> as seen in Figure 4. For beams slower than  $f/6.3$  the scattering becomes so large that the output beam never contains more light than the input beam for any angle.

### 2.4.2 Wavelength Dependence and Total Throughput

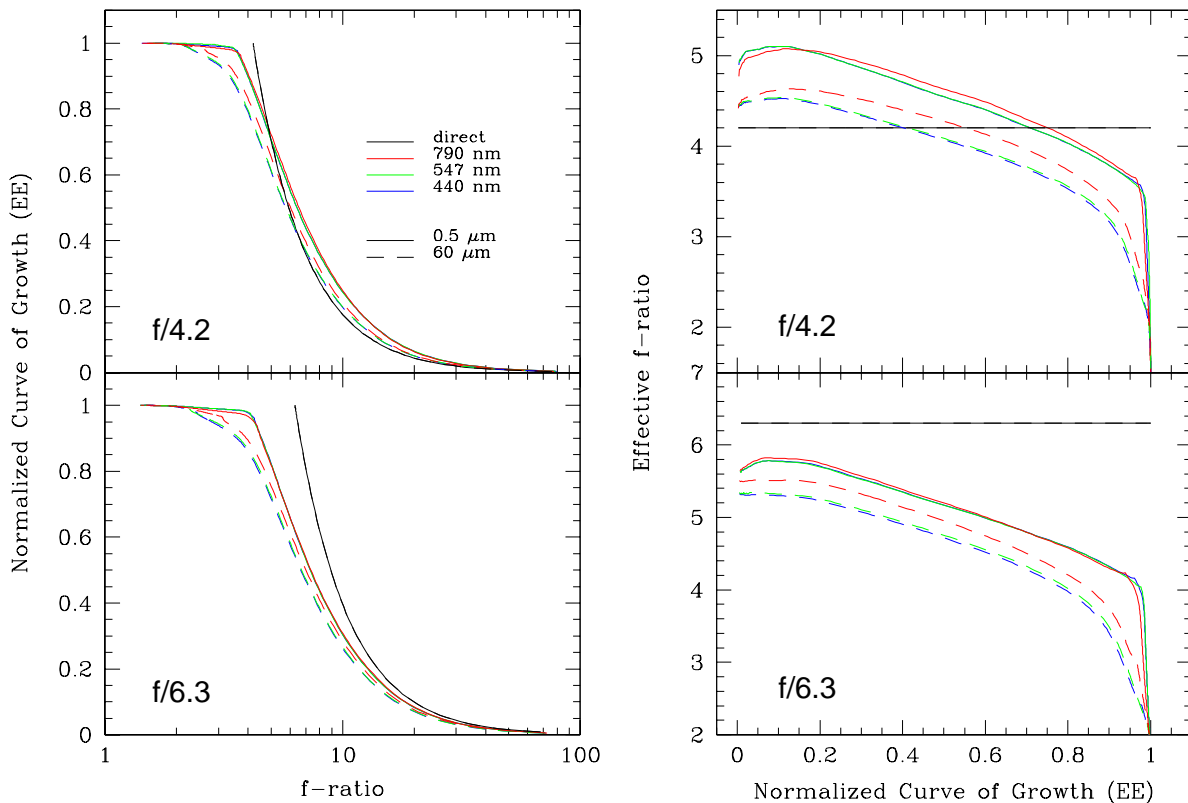


Figure 5. Wavelength dependence of FRD at 0.5 and 60  $\mu\text{m}$  polish grit at  $f/4.2$  and  $f/6.3$  for 17m length FBP300330370 fiber. A color version of this plot is available online.

Previous tests for a wavelength dependence on FRD have been split between results that suggest there is such a dependence,<sup>2,4</sup> based on what would be predicted by a micro-bend origin, and results that point to no wavelength dependence.<sup>8,10</sup> Figure 5 shows FRD curves for all filters at  $f/4.2$  and  $f/6.3$  and  $0.5 \mu\text{m}$  and  $60 \mu\text{m}$  polish levels. The data suggest that at a fine polish level ( $0.5 \mu\text{m}$ ) the amount of scattering caused by FRD does *not* depend on the wavelength of the input light. However, at  $60 \mu\text{m}$  we do see some wavelength dependence to the FRD curves, which must therefore be caused by surface scattering (see figure 6).

We also find that the total throughput of the fiber depends on fiber polish. Figure 6 shows the total throughput as a function of grit size for all three wavelengths and  $f/6.3$ . The total throughput is defined as the asymptotic (in output angle) fiber beam counts referenced to the same measurement of the direct beam. From the manufacturer’s specifications we expect the fiber attenuation to depend on wavelength. Polymicro reports attenuations of 20 dB/km at 440 nm, 10 dB/km at 551 nm, and 5 dB/km at 790 nm, and we also expect a 3.43% light loss from each air-silica interface (input and output faces). Thus, in the case of an ideal, 17 m long fiber we expect a throughput of 85.6%, 89.3%, and 91.2% for 440 nm, 551 nm, and 790 nm, respectively. These values are plotted as horizontal dashed lines in figure 6. Any additional losses are likely due to surface scattering.

We also find a polish dependence on the color of the transmission. As seen in the right panel of figure 6, the throughput gains are greater at shorter wavelengths as the surface-polish improves, as would be expected from a surface-scattering phenomenon.

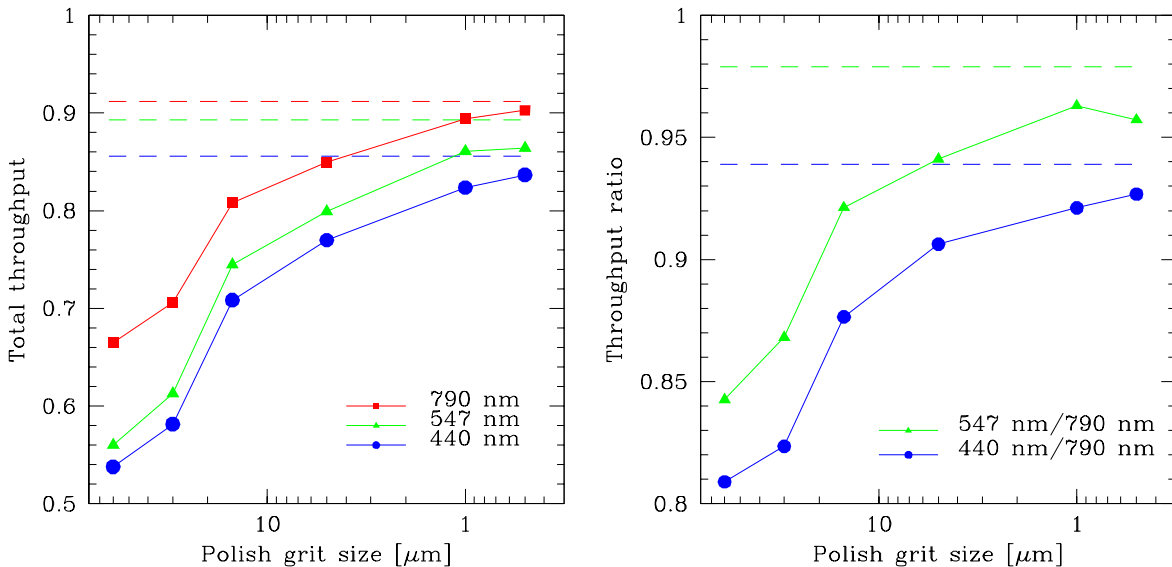


Figure 6. Total throughput as a function of polish grit for three different wavelengths (left), and the relative increase in 440 nm and 551 nm referenced to 790 nm (right). Dashed lines show the values expected from the product specifications. This is measured for a 17m length of FBP400440480 fiber. A color version of this plot is available online.

### 3. ANGLE DEPENDENCE

#### 3.1 Experiment

We are also interested in the dependence of FRD on the light input angle. The direct beam injection method reported in §2.2 injects a full cone of light into a fiber, i.e., the input beam contains rays incident on the fiber face from normal up to half of the vertex angle of the cone. To probe FRD effects at single, discrete input angles (essentially an annular cone) we use an experiment similar to the laser injection method of Carrasco and Parry (1994),<sup>2,5</sup> but modified so that the far field fiber output is imaged on to an opaque screen rather than through

a translucent screen. This was done to eliminate ring blurring that occurs when imaging through a translucent object of finite thickness.

We also needed to ensure that the imaging screen was far enough away from the output fiber face. The output images consist of a ring with a radius corresponding to the laser input angle and a thickness that varies depending on the amount of FRD present at that particular input angle. We expect each ring to have an inherent width equal to the diameter of the fiber, but this width is in a collimated beam while any FRD scattering results in a slightly diverging beam. With this in mind, the far field images were recorded at a far enough distance from the fiber output face that the FRD smearing width described by Carrasco and Parry (1994)<sup>2</sup> and Haynes et al. (2011)<sup>5</sup> (calculated to be  $\sim 2.6^\circ$  for our fiber) dominated the ring width. At the distance chosen the 300  $\mu\text{m}$  core of the fiber subtends  $\sim 0.06^\circ$  on the screen. Unfortunately, our direct-imaging approach requires the fiber output and camera to be off-axis (due to physical constraints), resulting in elliptical ring images. Significant effort was expended to model the geometric distortion caused by this method; our analysis software does an excellent job of removing the distortion to produce circular rings.

Data were taken at input angles of  $\pm 17^\circ$  ( $\sim f/1.6$ ) in increments of  $0.5^\circ$ . For simplicity we use the FWHM of the ring profile as a first-order measure of for the amount of FRD, ignoring here the intricacies of the profile shape.<sup>2,5</sup>

### 3.2 Results

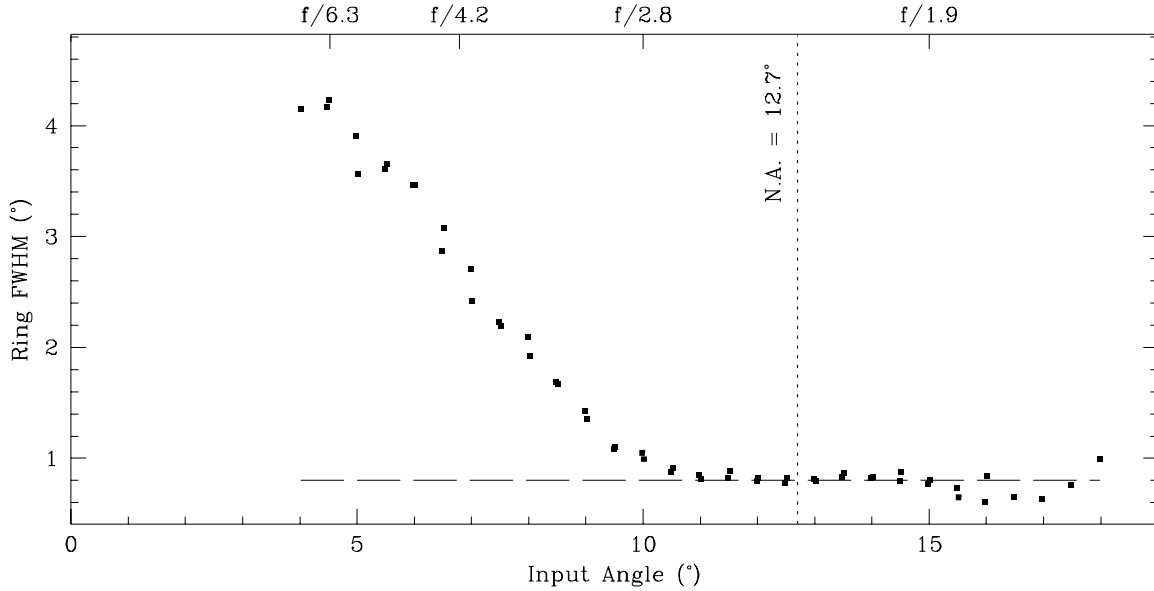


Figure 7. Smearing due to FRD (ring width) as a function on input angle. The vertical dotted line marks the numerical aperture of the fiber specified by the vendor. The horizontal dashed line represents a best fit to the micro-bend model of Carrasco and Parry 1994<sup>2</sup> over the full angular range of our data adopting  $D = 1.15 \times 10^{-6} \text{ m}^{-1}$ . This value of  $D$  is constrained by a best-fit of the micro-bend model to our data in the range of 10 to 18 degrees.

Figure 7 shows how the amount of “smearing” caused by FRD (ring width) varies with different input beam angles. Angles below  $4^\circ$  are not plotted; future reports of this experiment will measure ring widths in the regime where ring-width exceeds ring radius.

The results in figure 7 show that FRD effects are very large at small angles, as expected, and decrease with increasing angle until leveling out at  $\sim 10^\circ$ , which is within a few degrees of the numerical aperture ( $12.7^\circ$ ). It is possible to extend the ring measurements to angles above the numerical aperture. While the throughput decreases in this regime, the FRD appears to remain fairly constant.



We have compared these trends to predictions of the micro-bend model presented in Carrasco and Parry (1994).<sup>2</sup> We find a micro-bend parameter of  $D = 1.15 \times 10^{-6} \text{ m}^{-1}$  provides the best fit to our data (plotted in figure 7). This is a lower limit on the value of  $D$  for this fiber. An upper limit on the value of  $D$  comes from matching the micro-bend model to our widest ring ( $4^\circ$ ), from which we find  $D < 2.0 \times 10^{-5} \text{ m}^{-1}$ . For this range of  $D$ , our measurements are in an angular regime where the micro-bend model predicts a ring width nearly constant in angle. The fact that our data show a non-constant ring-width indicates that this micro-bend model is not a good description of the data and therefore not likely the physical origin of FRD.

Our results are also important because they indicate just how strongly FRD is dominated by light entering the fiber at smaller angles with respect to the fiber optical axis. In astronomical applications, fibers are typically fed by on-axis optical systems with central obstructions from secondary and/or field-corrector optics. From an entropy stand-point, i.e., information gathering-power per unit cost, the central rays obscured are the least valuable. Consequently, wide-field survey-telescopes (e.g., SDSS<sup>11,12</sup>), which are fast and have relatively large central obstructions, are ideally suited to fiber coupling. Further analysis of data like that in Figure 7 will allow us to quantify this statement.

#### 4. SUMMARY

Two experiments to measure the amplitude of FRD as a function of wavelength, surface polish, and light-injection angle have been carried out and described. The primary results are:

1. A component of FRD is attributable to the end-polish on fiber surfaces, however this appears to be a second-order effect relative to the impact of light-injection angle (beam speed) slower than  $f/3$ . FRD decreases with polishing down to finer grit sizes, but not significantly below grit-sizes of  $5 \mu\text{m}$ .
2. Total throughput (light emerging at all angles) also depends on end-polish, with a wavelength dependence that indicates the increase in throughput is simply a reduction in surface-scattering. The most significant gains occur for polishing that proceeds down to  $5 \mu\text{m}$  grit, although for most astronomical applications at low light-levels polishing down to the finest grit is measurably advantageous.
3. The amount of FRD does **not** depend on wavelength, as found now in several experiments. This is in contrast to some results and the predictions of micro-bend theory for FRD's origin.<sup>2</sup>
4. FRD is dominated by light entering the fiber at smaller angles (in our case  $< 10^\circ$ ), as is well known. Measurements here allow us to quantify this statement in detail. The amplitude and angular dependence of FRD also do not agree with predictions from micro-bend theory.

This work was supported by NSF grants ATI-0804576 and AST-1009471.

#### REFERENCES

1. J. R. P. Angel, M. T. Adams, T. A. Boroson, and R. L. Moore, "A very large optical telescope array linked with fused silica fibers," *The Astrophysical Journal* **218**, pp. 776–782, Dec. 1977.
2. E. Carrasco and I. R. Parry, "A method for determining the focal ratio degradation of optical fibres for astronomy," *MNRAS* **271**, p. 1, Nov. 1994.
3. A. C. de Oliveira, L. S. de Oliveira, J. B. Dos Santos, M. V. Arruda, L. G. C. Dos Santos, F. Rodrigues, and F. L. F. de Castro, "FRD in optical fibres at low temperatures: investigations for Gemini's Wide-field Fibre Multi-Object Spectrograph," *MNRAS* **413**, pp. 3003–3012, June 2011.
4. D. Gloge, "Bending loss in multimode fibers with graded and ungraded core index," *Appl. Opt.* **11**, pp. 2506–2513, Nov 1972.
5. D. M. Haynes, M. J. Withford, J. M. Dawes, J. S. Lawrence, and R. Haynes, "Relative contributions of scattering, diffraction and modal diffusion to focal ratio degradation in optical fibres," *MNRAS* **414**, pp. 253–263, June 2011.
6. G. Avila, "Results on Fiber Characterization at ESO," in *Fiber Optics in Astronomy III*, S. Arribas, E. Mediavilla, and F. Watson, eds., *Astronomical Society of the Pacific Conference Series* **152**, p. 44, 1998.

7. L. Crause, M. Bershad, and D. Buckley, "Investigation of focal ratio degradation in optical fibres for astronomical instrumentation," in *Society of Photo-Optical Instrumentation Engineers (SPIE) Conference Series, Presented at the Society of Photo-Optical Instrumentation Engineers (SPIE) Conference 7014*, Aug. 2008.
8. M. A. Bershad, D. R. Andersen, J. Harker, L. W. Ramsey, and M. A. W. Verheijen, "SparsePak: A Formatted Fiber Field Unit for the WIYN Telescope Bench Spectrograph. I. Design, Construction, and Calibration," *PASP* **116**, pp. 565–590, June 2004.
9. L. W. Ramsey, "Focal ratio degradation in optical fibers of astronomical interest," in *Fiber Optics in Astronomy*, S. C. Barden, ed., *Astronomical Society of the Pacific Conference Series* **3**, pp. 26–39, 1988.
10. J. Schmoll, M. M. Roth, and U. Laux, "Statistical Test of Optical Fibers for Use in PMAS, the Potsdam Multi-Aperture Spectrophotometer," *PASP* **115**, pp. 854–868, July 2003.
11. D. G. York, J. Adelman, J. E. Anderson, Jr., S. F. Anderson, J. Annis, N. A. Bahcall, J. A. Bakken, R. Barkhouser, S. Bastian, E. Berman, W. N. Boroski, S. Bracker, C. Briegel, J. W. Briggs, J. Brinkmann, R. Brunner, S. Burles, L. Carey, M. A. Carr, F. J. Castander, B. Chen, P. L. Colestock, A. J. Connolly, J. H. Crocker, I. Csabai, P. C. Czarapata, J. E. Davis, M. Doi, T. Dombeck, D. Eisenstein, N. Ellman, B. R. Elms, M. L. Evans, X. Fan, G. R. Federwitz, L. Fiscelli, S. Friedman, J. A. Frieman, M. Fukugita, B. Gillespie, J. E. Gunn, V. K. Gurbani, E. de Haas, M. Haldeman, F. H. Harris, J. Hayes, T. M. Heckman, G. S. Hennessy, R. B. Hindsley, S. Holm, D. J. Holmgren, C.-h. Huang, C. Hull, D. Husby, S.-I. Ichikawa, T. Ichikawa, Ž. Ivezić, S. Kent, R. S. J. Kim, E. Kinney, M. Klaene, A. N. Kleinman, S. Kleinman, G. R. Knapp, J. Korienek, R. G. Kron, P. Z. Kunszt, D. Q. Lamb, B. Lee, R. F. Leger, S. Limmongkol, C. Lindenmeyer, D. C. Long, C. Loomis, J. Loveday, R. Lucinio, R. H. Lupton, B. MacKinnon, E. J. Mannery, P. M. Mantsch, B. Margon, P. McGehee, T. A. McKay, A. Meiksin, A. Merelli, D. G. Monet, J. A. Munn, V. K. Narayanan, T. Nash, E. Neilsen, R. Neswold, H. J. Newberg, R. C. Nichol, T. Nicinski, M. Nonino, N. Okada, S. Okamura, J. P. Ostriker, R. Owen, A. G. Pauls, J. Peoples, R. L. Peterson, D. Petravick, J. R. Pier, A. Pope, R. Pordes, A. Prosapio, R. Rechenmacher, T. R. Quinn, G. T. Richards, M. W. Richmond, C. H. Rivetta, C. M. Rockosi, K. Ruthmansdorfer, D. Sandford, D. J. Schlegel, D. P. Schneider, M. Sekiguchi, G. Sergey, K. Shimasaku, W. A. Siegmund, S. Smee, J. A. Smith, S. Snedden, R. Stone, C. Stoughton, M. A. Strauss, C. Stubbs, M. SubbaRao, A. S. Szalay, I. Szapudi, G. P. Szokoly, A. R. Thakar, C. Tremonti, D. L. Tucker, A. Uomoto, D. Vanden Berk, M. S. Vogeley, P. Waddell, S.-i. Wang, M. Watanabe, D. H. Weinberg, B. Yanny, N. Yasuda, and SDSS Collaboration, "The Sloan Digital Sky Survey: Technical Summary," *The Astronomical Journal* **120**, pp. 1579–1587, Sept. 2000.
12. J. E. Gunn, W. A. Siegmund, E. J. Mannery, R. E. Owen, C. L. Hull, R. F. Leger, L. N. Carey, G. R. Knapp, D. G. York, W. N. Boroski, S. M. Kent, R. H. Lupton, C. M. Rockosi, M. L. Evans, P. Waddell, J. E. Anderson, J. Annis, J. C. Barentine, L. M. Bartoszek, S. Bastian, S. B. Bracker, H. J. Brewington, C. I. Briegel, J. Brinkmann, Y. J. Brown, M. A. Carr, P. C. Czarapata, C. C. Drennan, T. Dombeck, G. R. Federwitz, B. A. Gillespie, C. Gonzales, S. U. Hansen, M. Harvanek, J. Hayes, W. Jordan, E. Kinney, M. Klaene, S. J. Kleinman, R. G. Kron, J. Kresinski, G. Lee, S. Limmongkol, C. W. Lindenmeyer, D. C. Long, C. L. Loomis, P. M. McGehee, P. M. Mantsch, E. H. Neilsen, Jr., R. M. Neswold, P. R. Newman, A. Nitta, J. Peoples, Jr., J. R. Pier, P. S. Prieto, A. Prosapio, C. Rivetta, D. P. Schneider, S. Snedden, and S.-i. Wang, "The 2.5 m Telescope of the Sloan Digital Sky Survey," *The Astronomical Journal* **131**, pp. 2332–2359, Apr. 2006.